Journal of Engineering Mathematics 22: 335–354 (1988)

On numerical simulation of the continuous casting process

E. LAITINEN and P. NEITTAANMÄKI
Department of Mathematics, University of Jyväskylä, Seminaarinkatu 15, SF-40100 Jyväskylä, Finland

Received 10 November 1987; accepted 22 April 1988

Abstract. In this paper a steady-state nonlinear parabolic-type model, which simulates the multiphase heat transfer during solidification in continuous casting, is presented. An enthalpy formulation is used and we apply a FE-method in space and an implicit Euler method in time. A detailed solution algorithm is presented. We compute the temperature distributions in the strand when the boundary conditions (mold/spray cooling) on the strand surface are known. The numerical model gives thereby a good basis for the testing of new designs of continuous-casting machines. An application of the model to continuous casting of billets is presented.

1. Introduction

A considerable amount of the world's steel is now produced by the continuous casting process. The complexity of this process is such that until recently innovations to machine design could only be tested by full-scale runs on a production machine. This is extremely costly and in many cases production cannot be delayed to perform such tests. However, numerical simulation models of the continuous casting process have recently been developed [1, 7, 8, 14]. They offer an important alternative mean of testing new designs.

The essential features of a continuous-casting machine are shown in Figure 1. The molten steel is fed from a ladle into a water-cooled mold. The product is supported by rolls after mold and cooled down by water sprays during the secondary cooling region. After the end of secondary cooling (point z_2 in Fig. 1) the product is cooled down only by radiation. The unbending point and the cutting point are at distances z_4 and z_5 from the meniscus, respectively.

The rate at which the heat extraction proceeds is critical to the smooth operation of the process, because undercooling can result in excessively long liquid pools and overcooling can lead to the formation of cracks at the bending or straightening rolls. The heat extraction in the sprays must also be arranged such that there is a smooth transition of the surface temperature, with a minimum of reheating, as the steel passes from the mold to the sprays and from the sprays to the radiation-cooling zones. The aspect of the spray design will be discussed in more detail in a forthcoming paper.

The first step in the numerical simulation of the continuous-casting system is to have a modified model for the heat equation with a moving boundary (liquid/solid). The main difficulty is that the position of the moving boundary is not known and depends on the variables which are to be solved. Such problems are usually known as Stefan problems or moving-boundary problems. Furthermore, there exists a discontinuity in the moving boundary: due to the effect of latent heat the temperature gradient across the solid/liquid interface is discontinuous. For analytical and numerical approaches for Stefan-type problems we refer to [2–5, 11, 13, 16–20].

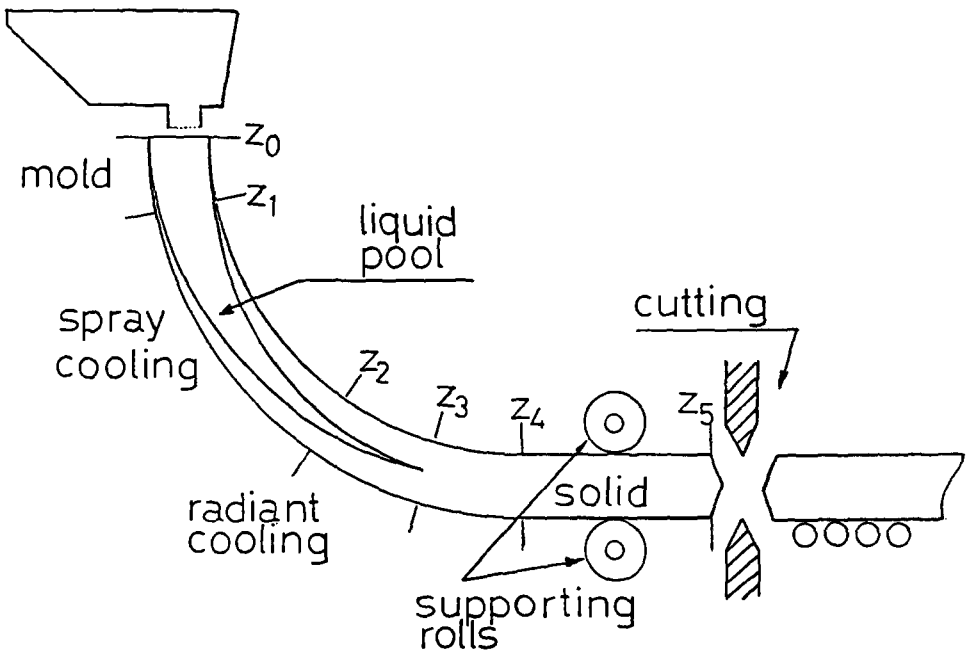

Fig. 1. Schematic representation of the continuous casting process; z_i distance from the meniscus.

Our situation requires solutions of the heat equation with phase transitions, the location of which is not a-priori known. Moreover, the boundary conditions are nonlinear. This makes the solution algorithm quite complicated. This paper is organized as follows: first we shall shortly derive the parabolic-type heat-conduction equation, the solution of which gives the temperature distribution during the casting process. The variational formulation, which is a basis of the FE-approximation, is given in Section 2. In Section 4 we present a detailed solution algorithm for the problem in question. The algorithm does not need any a-priori knowledge about the position of the moving boundary. Only the temperature of liquid metal at the top of the mold and the cooling conditions are needed. Finally, in Section 6, several numerical examples are presented. As a by-product of our result, we give a simple algorithm (with numerical test) for the inverse problem, by means of which one can determine the cooling conditions when a desired surface temperature is given (Section 7).

2. The mathematical simulation model for the temperature distribution in a continuous-casting machine

2.1. The enthalpy formulation

The heat transfer from the interior of the strand cross-section $\Omega \subset R^2$ to the external surface Γ is assumed to be described by means of Fourier's law. The nonlinear heat-conduction equation can be written in the form

$$\varrho(T)c(T)\frac{\partial}{\partial t}T = \operatorname{div}(k(T)\nabla T) + q. \tag{1}$$

Here $T = T(x, t)$ is the temperature in a point $x \in \Omega$ at time t; $q = q(T)$ constitutes a source term corresponding to heat being emitted or absorbed; $q = 0$ everywhere except in the mushy region where latent heat is emitted. Furthermore $c(T)$ denotes the specific heat, $\varrho(T)$ the density and $k(T)$ is the thermal conductivity. The geometry of the cross-section Ω can be, for example, a square, a rectangle (they may have rounded corners, as well) or a circle.

When local freezing in a mushy zone (temperature range $[T_s, T_l]$) is occurring, the associated latent heat L constitutes a heat source, which is taken care of by the source term q in equation (1). By applying an expression $f_s = f_s(T)$ which describes how the solid-phase fraction varies with temperature, q can be expressed in accordance with equation (2):

$$q(T) = \varrho L \frac{\partial f_s}{\partial T} \frac{\partial T}{\partial t}. \tag{2}$$

In practice, the form of the f_s versus T curve depends primarily on local solute redistribution. To keep the solution algorithm in Section 4 simple, we assume that f_s varies linearly between solidus temperature T_s and liquidus temperature T_l. Then the following relation is obtained:[1]

$$\frac{\partial f_s}{\partial T} = -\frac{1}{T_l - T_s}; \quad T_l \geqslant T_s. \tag{3}$$

If equation (3) is integrated with respect to temperature between the limits T_s and T_l, the value 1 is obtained. By equations (1)–(3) we get the heat-transfer model

$$\left[\varrho(T)c(T) + \frac{\varrho(T)L}{T_l - T_s}\right] \frac{\partial}{\partial t} T(x, t) = \operatorname{div}[k(T)\nabla T]. \tag{4}$$

The heat transfer from the strand surface to the environment is assumed to take place by convection, conduction and radiation. We have the boundary conditions (5)–(7) when we assume that heat is extracted by convection and conduction in the *mold-cooling region*,

$$-k(T) \frac{\partial}{\partial n} T = h_{\text{mold}}(T - T_{\text{mold}}) \quad \text{in the mold region,} \tag{5}$$

by convection and radiation in the *secondary cooling region*,

$$-k(T) \frac{\partial}{\partial n} T = h(T - T_{\text{H}_2\text{O}}) + \sigma\varepsilon(T^4 - T_{\text{ext}}^4) \quad \text{in the secondary cooling region,} \tag{6}$$

and by radiation only in the *radiant cooling region*,

$$-k(T) \frac{\partial}{\partial n} T = \sigma\varepsilon(T^4 - T_{\text{ext}}^4) \quad \text{in the radiant cooling region.} \tag{7}$$

[1] The form of f_s in the mushy zone depends strongly on steel analysis, and the assumed linearity of f_s is the most contentious aspect of the mathematical model. The form of f_s can be determined experimentally (in recent years it has also been determined mathematically) and there is a large metallurgical literature on the subject, starting with the Scheil equation. The solving algorithm presented in Section 4 is easily extended to the case where f_s varies piecewise linearly in the mushy zone (see Fig. 2).

Here T_{mold} is the ambient temperature, h_{mold} and h are the heat-transfer coefficients in the mold and in the secondary cooling region, resp., T_{H_2O} is the spray-water temperature, T_{ext} is the ambient spray/radient zone temperature, σ is Stefan–Boltzmann constant and ε is the emission factor.

When pouring is commenced, the melt is assumed to have a temperature T_l. Then the initial condition can be written as

$$T(x, 0) = T_l; \quad x \in \Omega. \tag{8}$$

We shall use an enthalpy formulation for problem (4)–(8). To do this we shall define new variables: the enthalpy

$$H(T) = \int_0^T \left[\varrho(\xi)c(\xi) + \frac{\varrho(\xi)L}{T_l - T_s} \right] \mathrm{d}\xi \tag{9}$$

and the Kirchhoff transform

$$K(T) = \int_0^T k(\xi)\, \mathrm{d}\xi, \tag{10}$$

which both are smooth functions of temperature.

According to (4), (9), (10) and (5)–(8), our mathematical simulation model for the temperature distribution $T = T(x, t)$ during the casting process can be written as follows:

$$\frac{\partial}{\partial t} H(T) = \Delta K(T) \qquad \text{in } \Omega \times]0, t_5[, \tag{11}$$

$$-k(T) \frac{\partial}{\partial n} T = \begin{cases} h_{\text{mold}}(T - T_{\text{mold}}) & \text{in } \Gamma \times]0, t_1], \\ h(T - T_{H_2O}) + \sigma\varepsilon(T^4 - T_{\text{ext}}^4) & \text{in } \Gamma \times]t_1, t_2], \\ \sigma\varepsilon(T^4 - T_{\text{ext}}^4) & \text{in } \Gamma \times]t_2, t_5[, \end{cases} \tag{12}$$

$$T(x, 0) = T_l(x) \qquad \text{in } \Omega. \tag{13}$$

2.2. The variational formulation for model (11)–(13)

In order to use the Hilbert-space setting of problem (11)–(13), we introduce appropriate function spaces. Let $L^2(\Omega)$ be the set of square-integrable functions with norm

$$\|v\| = \left[\int_\Omega (v(x))^2 \, \mathrm{d}x \right]^{1/2}$$

and scalar product

$$(u, v) = \int_\Omega u(x)v(x) \, \mathrm{d}x.$$

Let $H^1(\Omega)$ be the Sobolev space of order 1:

$$H^1(\Omega) = \left\{ v \in L^2(\Omega) \mid \frac{\partial}{\partial x_i} v \in L^2(\Omega),\ i = 1, 2 \right\}.$$

Furthermore, we introduce the bilinear form

$$a(u, v) = \sum_{i=1}^{2} \left(\frac{\partial}{\partial x_i} u, \frac{\partial}{\partial x_i} v \right)$$

and the $L^2(\Gamma)$-scalar product $\langle \cdot, \cdot \rangle$,

$$\langle u, v \rangle = \int_\Gamma u(x) v(x)\, d\Gamma,$$

where $\Gamma = \partial\Omega$.

Multiplying equation (11) by a smooth function $v \in H^1(\Omega)$ and using Green's theorem and equation (12) we obtain the variational formulation for problem (11)–(13): find $H(T) \in L^2(\Omega \times]0, t_5[)$ with $T(x, t) \in L^2(H^1(\Omega);]0, t_5[)$ satisfying for all $v \in H^1(\Omega)$ the relations:

$$\left(\frac{\partial}{\partial t} H(T), v \right) + a(K(T), v) = -\langle h_{\text{mold}}(x, t)(T - T_{\text{mold}}), v \rangle \quad \text{in } \Omega \times]0, t_1], \tag{14}$$

$$\left(\frac{\partial}{\partial t} H(T), v \right) + a(K(T), v) = -\langle h(x, t)(T - T_{H_2O}), v \rangle - \sigma\varepsilon \langle T^4 - T_{\text{ext}}^4, v \rangle \quad \text{in } \Omega \times]t_1, t_2], \tag{15}$$

$$\left(\frac{\partial}{\partial t} H(T), v \right) + a(K(T), v) = -\sigma\varepsilon \langle T^4 - T_{\text{ext}}^4, v \rangle \quad \text{in } \Omega \times]t_2, t_5[, \tag{16}$$

$$T(x, 0) = T_l \quad \text{in } \Omega. \tag{17}$$

The results concerning existence, uniqueness and stability of weak solutions of problem (11)–(13) can be distinguished according to types of hypotheses on the nonlinear flux term, such as regularity, monotonicity assumptions, growth conditions and bounds. A survey on the results available for weak formulations of the nonlinear Stefan problem in the multi-dimensional case is given in [11].

3. Approximation of the problem (14)–(17)

In the approximation scheme the weak formulation (14)–(17) of the problem (11)–(13) is used. The discretization is performed by finite elements (piecewise linear) in space and by finite differences in time.

We consider a family $\mathcal{T}_d$ of regular triangulations consisting of triangles with vertices lying on $\bar{\Omega}$. To each $\mathcal{T}_d$ we associate a finite-element space (d is discretization parameter)

$$V_d = \{ v \in C^0(\bar{\Omega}) \mid v \text{ is linear on every element of } \mathcal{T}_d \}.$$

Let L_d be the space of traces of functions from V_d on $\partial\Omega$. Denote $n = \dim(V_d)$ and $p = \dim(L_d)$ where $p < n$. Let $\{x_j\}_{j=1}^n$ be the set of all nodes of $\mathcal{T}_d$ and suppose $\{x_j\}_{j=1}^p$ is the set of nodes lying on Γ. By $v_j(x) \in V_d$ we denote the basis functions (Courant's basis functions) associated with the node x_j:

$$v_j(x_k) = \begin{cases} 1, & \text{if } k = j; \\ 0, & \text{if } k \neq j. \end{cases}$$

We consider the uniform (Δt_i the timestep) partition of the intervals $[0, t_1]$, $[t_1, t_2]$ and $[t_2, t_5]$:

$$0 = t^0 < t^1 < \cdots < t^{N_1-1} < t^{N_1} = t_1 < t^{N_1+1} < \cdots < t^{N_2}$$

$$= t_2 < t^{N_2+1} < \cdots < t^{N_5} = t_5.$$

The discretization of the problem (14)–(17) consists of using backward differences in time, and of linear elements in space. From (14)–(17) we thus get the nonlinear system for finding T_d^{i+1}:

$$\left(\frac{H(T_d^{i+1}) - H(T_d^i)}{\Delta t_1}, v\right) + a(K(T_d^{i+1}), v) + \langle h_{\text{mold}}^{i+1} T_d^{i+1}, v\rangle = \langle h_{\text{mold}}^{i+1} T_{\text{mold}}, v\rangle$$
$$\text{for all } v \in V_d,\ i = 1, \ldots, N_1; \tag{18}$$

$$\left(\frac{H(T_d^{i+1}) - H(T_d^i)}{\Delta t_2}, v\right) + a(K(T_d^{i+1}), v) + \langle h^{i+1} T_d^{i+1}, v\rangle = \sigma\varepsilon\langle (T_d^4)^{i+1}, v\rangle$$

$$= \langle h^{i+1} T_{\text{H}_2\text{O}}^{i+1}, v\rangle + \sigma\varepsilon\langle (T_{\text{ext}}^4)^{i+1}, v\rangle \quad \text{for all } v \in V_d,\ i = N_1, \ldots, N_2; \tag{19}$$

$$\left(\frac{H(T_d^{i+1}) - H(T_d^i)}{\Delta t_3}, v\right) + a(K(T_d^{i+1}), v) + \sigma\varepsilon\langle (T_d^4)^{i+1}, v\rangle = \sigma\varepsilon\langle (T_{\text{ext}}^4)^{i+1}, v\rangle$$
$$\text{for all } v \in V_d,\ i = N_2 + 1, \ldots, N_5; \tag{20}$$

$$T_d^0 = T_l. \tag{21}$$

The finite-element approximation $T_d^i \in V_d$ of the temperature T at time $t = t^i$ has the form

$$T_d^i(x) = \sum_{j=1}^n T_j^i v_j(x), \tag{22}$$

where $T^i = (T_1^i, \ldots, T_n^i)$ is the nodal-value vector of $T_d^i(x)$. Supposing that H and K are piecewise linear in T we obtain interpolation expressions at time $t = t^i$

$$H(T_d^i) = \sum_{i=1}^n H(T_j^i) v_j(x); \quad K(T_d^i) = \sum_{i=1}^n K(T_j^i) v_j(x). \tag{23}$$

In order to approximate the integrals appearing the following quadrature formula for the N-dimensional simplex S is chosen:

$$I_S(F) = \frac{\text{meas}\,(S)}{N+1} \sum_{i=1}^{N+1} F(x^i),$$

where x^i are vertices of S. Then we introduce the approximations

$$(w, v) \approx (w, v)_d = \sum_{K \in \mathcal{T}_d} I_K(wv); \quad a(w, v) \approx a(w, v)_d = \sum_{K \in \mathcal{T}_d} I_K(\nabla\omega\nabla v);$$

$$\langle w, v\rangle \approx \langle w, v\rangle_d = \sum_{\substack{K \in \mathcal{T}_d \\ K \cap \partial\Omega \neq 0}} I_{K \cap \partial\Omega}(wv).$$

Setting $v = v_j$, $j = 1, \ldots, n$ in equations (18)–(21) we see that the computation of the nodal temperature vector T^{i+1}, at time level t^{i+1}, $i = 0, \ldots, N-1$ is equivalent to the solution of the nonlinear system

$$M \frac{H(T^{i+1}) - H(T^i)}{\Delta t_1} + AK(T^{i+1}) + B(h^{i+1}_{\text{mold}})T^{i+1} = B(h^{i+1}_{\text{mold}})T^{i+1}_{\text{mold}}, \quad i = 1, \ldots, N_1; \tag{24}$$

$$M \frac{H(T^{i+1}) - H(T^i)}{\Delta t_2} + AK(T^{i+1}) + B(h^{i+1})T^{i+1} + \sigma\varepsilon B T^{i+1^4}$$

$$= B(h^{i+1})T^{i+1}_{H_2O} + \sigma\varepsilon B T^{i+1^4}_{\text{ext}}, \qquad i = N_1 + 1, \ldots, N_2; \tag{25}$$

$$M \frac{H(T^{i+1}) - H(T^i)}{\Delta t_3} + AK(T^{i+1}) + \sigma\varepsilon B T^{i+1^4} = \sigma\varepsilon B T^{i+1^4}_{\text{ext}}, \qquad i = N_2 + 1, \ldots, N_5; \tag{26}$$

$$T^0 = T_l. \tag{27}$$

The matrices M, A, B are constant $n \times n$ band matrices, M and A are positive definite and B is positive semidefinite. The matrices M (mass matrix) and A (stiffness matrix) are defined as

$$M = \{(v_i, v_j)_d\}_{j,i=1}^n, \quad A = \{a(v_i, v_j)_d\}_{j,i=1}^n.$$

Moreover, $B = (b_{ij})$ is defined as follows:

$$b_{ij} = \begin{cases} d, & i = j = 1, \ldots, p, \\ 0, & \text{otherwise}, \end{cases}$$

where d denotes the mesh parameter on the boundary Γ. The notation $B(h)$ denotes the diagonal matrix with components

$$B(h)_{ij} = \begin{cases} dh_i, & i = j = 1, \ldots, p, \\ 0, & \text{otherwise.} \end{cases}$$

4. An algorithm for solving the system (24)–(27)

In order to solve equations (24)–(27) we use iterative methods. In the system (24)–(27) the nonlinearities are on the boundary Γ due to the nonlinear Stefan radiation condition and in the interior of Ω due to the nonlinear material properties. However, for simplicity, we assume that the material constants ϱ, c and k are piecewise constant functions of the temperature T. It implies (see (9), (10)) that the functions $H(T)$ and $K(T)$ are piecewise linear continuous functions of T. Hence, we are dealing with an implicitly linear system in the mold region $]0, t_1]$ and in the interior of Ω in the spray $]t_1, t_2]$ and radiant $]t_2, t_5[$ cooling region. Assuming furthermore, that the strand surface in spray and radiant cooling region is in the solid state, we can apply efficiently the combination of modified S.O.R. and Newton-Raphson method.

Assuming (for example) that the material properties are defined for three different temperature ranges $T < T_s$ (solidus temp.), $T_s \leqslant T \leqslant T_l$ (liquidus temp.) and $T > T_l$ then

$$H(T) = \begin{cases} H_s T + c_s, & T \leqslant T_s \\ H_m T + c_m, & T_s < T < T_l \\ H_l T + c_l, & T \geqslant T_l \end{cases}$$

$$K(T) = \begin{cases} K_s T + d_s, & T \leqslant T_s \\ K_m T + d_m, & T_s < T < T_l \\ K_l T + d_l, & T \geqslant T_l. \end{cases} \tag{29}$$

Moreover, metallurgically it is reasonable to demand that the cast has a solidifying shell when it leaves the mold. Hence the choice of the solution methods of systems (24)–(27) depends on the boundary data, that is, boundary-conditions type (linear/nonlinear) and the phase of boundary (known/unknown). Table 1 summarizes the situation. When using the Newton–Raphson method, the solution $T^{i+1} = (T_1^{i+1}, \ldots, T_n^{i+1})$ can be computed at time level $i + 1$ from the solution T^i of the previous time level i. The calculation is made component by component according to the iterative procedure

$$T_k^{i+1/2} = \begin{cases} T_k^i - \dfrac{F_k - \hat{m}_{kk} H_k^i - a_{kk} K_k^i - B(h^{i+1})_{kk} T_k^i - \varepsilon\sigma b_{kk} T_k^{i4}}{-\hat{m}_{kk} H_s - a_{kk} K_s - B(h^{i+1})_{kk} - 4\varepsilon\sigma b_{kk} T_k^{i3}}, & i = N_1 + 1, \ldots, N_2 \\ T_k^i - \dfrac{F_k - \hat{m}_{kk} H_k^i - a_{kk} K_k^i - \varepsilon\sigma b_{kk} T_k^{i4}}{-\hat{m}_{kk} H_s - a_{kk} K_s - 4\varepsilon\sigma b_{kk} T_k^{i3}}, & i = N_2 + 1, \ldots, N_5 \end{cases} \tag{30}$$

Table 1.

	$]0, t_1]$ Mold region	$]t_1, t_5[$ Sec./rad. cool. region
Governing equation	Implicitly linear	Implicitly linear
Boundary condition	Linear	Nonlinear
Phase on boundary Γ	Unknown	Solid
Phase on interior Ω	Unknown	Unknown
Method for solving eq. on Γ	Modified S.O.R.	Newton-Raphson
Method for solving eq. on Ω	Modified S.O.R.	Modified S.O.R.

where

$$F_k = \begin{cases} (\hat{M}H(T^i) + B(h^{i+1})T^{i+1}_{H_2O} + \sigma\varepsilon BT^{i+1^4}_{ext})_k - Q_k, & i = N_1 + 1, \ldots, N_2 \\ (\hat{M}(HT^i) + \sigma\varepsilon BT^{i+1^4}_{ext})_k - Q_k, & i = N_2 + 1, \ldots, N_5 \end{cases} \tag{31}$$

and

$$Q_k = \sum_{j=1}^{k-1} (\hat{m}_{kj}H(T_j^{i+1}) + a_{kj}K(T_j^{i+1})) + \sum_{j=k+1}^{n} (\hat{m}_{kj}H(T_j^i) + a_{kj}K(T_j^i)).$$

Here we have denoted $\hat{M} = (\hat{m}_{ij}) = m_{ij}/\Delta t_l$ where $l = 1, 2, 3$ depending on the value of time $t \in]0, t_1]$, $t \in]t_1, t_2]$ or $t \in]t_2, t_5[$, respectively.

In the mold region and in the interior of Ω along the secondary cooling region we apply the modified S.O.R. method. Because it is not a priori known where the free boundary lies in the interior of Ω, we must first test the value of F_k in the algorithm which indicates in what phase (solid, mushy, liquid) the computed node temperature T_k^{i+1} will be. According to this test we can choose the right values of $H(T)$ and $K(T)$ in the algorithm. Assuming that T^i is known, then T^{i+1} can be calculated using modified S.O.R. component by component according to the following iterative procedure:

$$T^{i+1/2} = \begin{cases} \dfrac{F_k - \hat{m}_{kk}c_s - a_{kk}d_s}{\hat{m}_{kk}H_s + a_{kk}K_s + B(h^{i+1}_{mold})_{kk}}, & \text{if} \\ F_k < (\hat{m}_{kk}H_s + a_{kk}K_s + B(h^{i+1}_{mold})_{kk}) \cdot T_s + \hat{m}_{kk}c_s + a_{kk}d_s; & \\ \dfrac{F_k - \hat{m}_{kk}c_l - a_{kk}d_l}{\hat{m}_{kk}H_l + a_{kk}K_l + B(h^{i+1}_{mold})_{kk}}, & \text{if} \\ F_k > (\hat{m}_{kk}H_l + a_{kk}K_l + B(h^{i+1}_{mold})_{kk}) \cdot T_l + \hat{m}_{kk}c_l + a_{kk}d_l; & \\ \dfrac{F_k - \hat{m}_{kk}c_m - a_{kk}d_m}{\hat{m}_{kk}H_m + a_{kk}K_m + B(h^{i+1}_{mold})_{kk}}, & \text{elsewhere,} \end{cases} \tag{32}$$

where

$$F_k = (\hat{M}H(T^i) + B(h^{i+1}_{mold})T^{i+1}_{mold})_k - Q_k. \tag{33}$$

So we get the algorithm:

ALGORITHM 1: (for solving (24)–(27))

STEP 0. Set $T^i := T^0$, $ite := 0$.

STEP 1. Set $ite := ite + 1$, $k := 0$.

STEP 2. Set $k := k + 1$.

STEP 3. If $i \in \{0, \ldots, N_1\}$ or $x_k \notin \Gamma$ then solve $T^{i+1/2}$ from equation (32) else solve $T^{i+1/2}$ from equation (30).

STEP 4. Set $T_k^{i+1} = T_k^i + \omega(T_k^{i+1/2} - T_k^i)$, $\omega \in]1.0, 1.85]$ an appropriate relaxation parameter.

STEP 5. If $k < n$ goto STEP 2.

STEP 6. If $|T_k^{i+1} - T_k^i| < \varepsilon|T_k^i| \; \forall k = 1, \ldots, n$ then STOP else set $T^i := T^{i+1}$.

STEP 7. If $ite < itemax$ goto STEP 1 else STOP.

5. Testing of the heat-transfer model

The difficulties associated with direct measurements on moving castings have made determination of solidification rates and temperature distributions difficult. An alternative approach is to simulate heat transfer mathematically in a continuously-cast section and calculate the temperature distribution as a function of the controllable variables of the process. For that purpose the previous ideas and algorithms were implemented into a Fortran 77 - coded computer program on a VAX 8600 under the VMS operating system. The program has roughly the following modular structure:

- *preprosessor:* FE-mesh generation and efficient storing of the sparse matrices M and A. Only the nonzero elements of matrices are allocated.
- *boundary and cast data generation:* the user assigns the boundary condition by forming an input file which includes the desired data.
- *implementation of the algorithms:* The discrete solutions for temperature distribution and/or heat-transfer coefficients are calculated and stored in files in view of their graphic treatment.
- *postprocessor:* The graphic representation of the discrete solutions. For the graphic outputs GPGS-F or DISSPLA graphic libraries are used.

In this section the continuous cast of steel billets is demonstrated.

5.1. The basic assumptions of the heat-transfer model

The schematic representation of the continuous casting process in Figure 1 illustrates that the strand passes through three distinct regions of cooling. Accordingly, the mathematical model consists of three parts:

(1) solidification in the mold,
(2) solidification in the spray cooling region,
(3) solidification in the radiant cooling region.

The heat-transfer model is based on the numerical solution of the equations (11)–(13). The model is simplified to a two-dimensional one because in continuous casting of steel the heat conduction in the withdrawal direction is minute and can be neglected. The specific heat

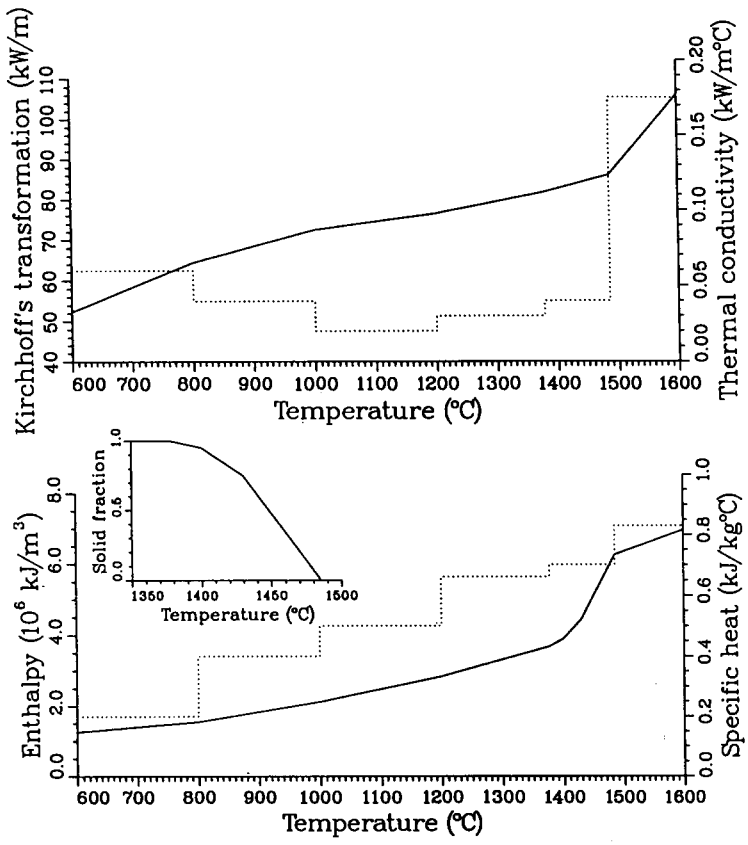

Fig. 2.

$c(T)$ and the thermal conductivity $k(T)$ of steel are defined separately for several different temperature regions, inside which they are assumed to be constant (Fig. 2). These assumptions imply by equations (9) and (10) that $H(T)$ and $K(T)$ are piecewise linear functions of T as indicated in Figure 2. Moreover, the solid fraction $f_s(T)$ is assumed to vary piecewise linearly between solidus and liquidus temperature (Fig. 2).

The convective heat flow in the liquid pool is quite complex due to the turbulent mixing imparted by the input metal stream. It is taken into account in the model by defining an effective liquid thermal conductivity, which includes the effects of convective mixing. It is assumed to be roughly six times greater than the normal value of the liquid thermal conductivity.

In order to solve equation (11) for the transient temperature distribution, boundary conditions as well as an initial condition must be specified. The specification of boundary conditions is done separately for the three distinct parts: mold, spray region and radiant cooling region. A schematic representation of defining boundary conditions is presented in Figure 3.

Mold. Heat transfer in the mold is governed by a series of three resistances: the casting/mold interface, the mold wall and the mold/cooling-water interface. The thermal resistance of the mold wall and mold/cooling-water interface as usually quite small compared with the

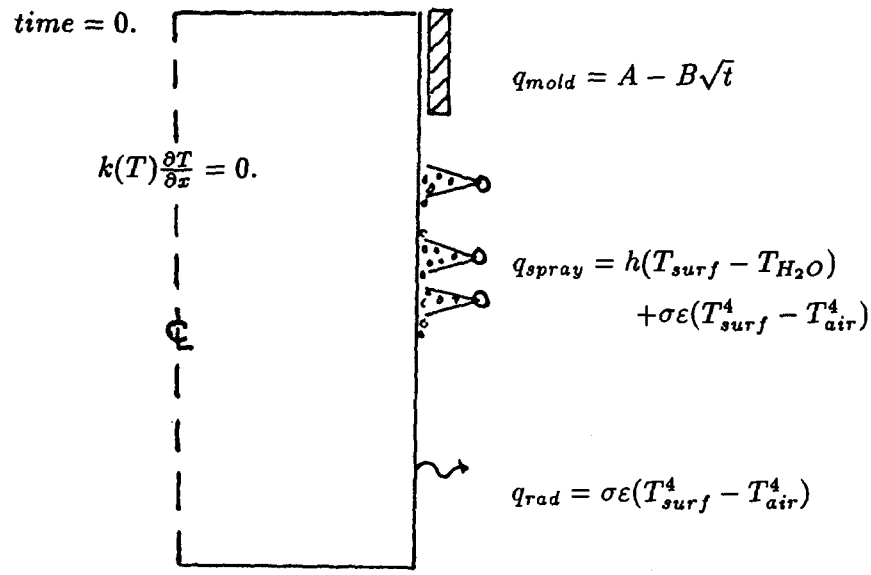

Fig. 3. Schematic representation of the boundary conditions in one half of the strand centre plane.

thermal resistance between the casting and mold, which consequently controls the rate of heat transfer in the mold.

For the case of billet casting we have used the following approximation for h_{mold}:

$$h_{\text{mold}}(x, t) = \begin{cases} 1.5 - 0.3\sqrt{\max(0, t - 9.6)}\ \dfrac{kW}{m^2\,^\circ K}, & x \text{ lies in the midface;} \\ 1.5 - 0.3\sqrt{\max(0, t - 6.4)}\ \dfrac{kW}{m^2\,^\circ K}, & x \text{ lies in the corner;} \\ \text{parabolic fitting of the above values for other } x. \end{cases} \tag{34}$$

Water-spray region. The purpose of the water-spray cooling is to continue the heat extraction and solidification initiated in the mold without generating tensile stresses of sufficient magnitude to cause shape defects, surface cracks or initial cracks. The spray chamber consists of spray nozzles positioned between support rolls. Four individual heat-transfer mechanisms, which act consecutively and/or in parallel, can be distinguished:

- direct spray cooling
- convective cooling by drainage water and by the vaporous atmosphere
- radiation and
- conduction to the support roller during contact.

In contrast to the mold cooling, the spray system is more flexible, from the standpoint of controlling the rate of heat removal from the strand. Thus it is relatively easy to achieve a desired temperature distribution in the strand by controlling the water pressure of the spray nozzles. For the adjust of spray-water pressure and quantity a group of nozzles are linked together forming a spray zone.

To carry out the spray design a stage further and transform heat-transfer coefficients ($\text{kWm}^{-2}(^\circ\text{K})^{-1}$) into spray-water flux profiles measured in $\text{lm}^{-2}\,\text{s}^{-1}$, empirical data relating

to the two variables must be available. That is, water pressure, nozzle type and stand-off distance affect h mainly through their effect on W.

Of course the relationship h versus W depends on casting conditions like strand size, machine design etc. However, this relationship is easy calculated for a caster using the inverse-temperature model with empirically measured Dirichlet boundary data and solving the corresponding heat-transfer coefficients h from the Neumann boundary condition by relation (6) (see Section 7).

Radiation zone. Radiation according to Stefan's law is the dominant cooling mechanism in this zone although some account is taken of the spray water which runs down the strand from the secondary cooling zone above.

Above we have defined the general principles concerning the boundary data and casting conditions in the simulation model of continuous casting. These principles are the same for the billet and slab casters.

6. Results of numerical tests

Consider the case of billet casting. The numerical values of material and casting data are shown in Table 2 and in Figure 2. The geometry of the billet's cross-section is approximately square with rounded corners (radius 5 mm) and the water cooling is assumed to be organised symmetrically along each of the billet's faces. Hence, for computational efficiency, we can use only one quarter of the billet's cross-section when we solve the problem. We approximate the nozzles water-flux distribution along the billet's horizontal side by a parabola (the corner region needs less cooling than the billet's midface). See Figure 4 for the representation of the geometry and approximation of the water-flux values at a fixed distance along the strand. One empirical water-flux measurement for a billet caster in l/(dm^2 min) is shown in Figure 5. The shadowed area of the bars in Figure 5 indicates the difference of water-flux values between corner and midface.

To solve the temperature distribution in the billet with the data given above, the water-flux values must be transformed into heat-transfer coefficients. Doing this, we use the relationship

$$h(x, t) = 0.13 \times W(x, t) + 0.1. \tag{35}$$

Figure 6 shows the corresponding heat-transfer coefficients in the secondary cooling region and the approximation of heat extraction in the mold according to equation (34).

Table 2. Material and casting data used

Carbon content	0.5%	ϱ	7200 kg/m^3
$T_l = T_0$	1485 °C	L	272 kJ/kg
T_s	1377 °C	σ	5.67×10^{-8} W/m^{2}K^4
T_{mold}	80 °C	ε	0.8
T_{H_2O}	27 °C	Cross-section: 100 × 100 mm^2	
T_{ext} spray zone	97 °C	Casting speed 2.80 m/min	
T_{ext} rad. zone	437 °C	Mold length 0.61 m	

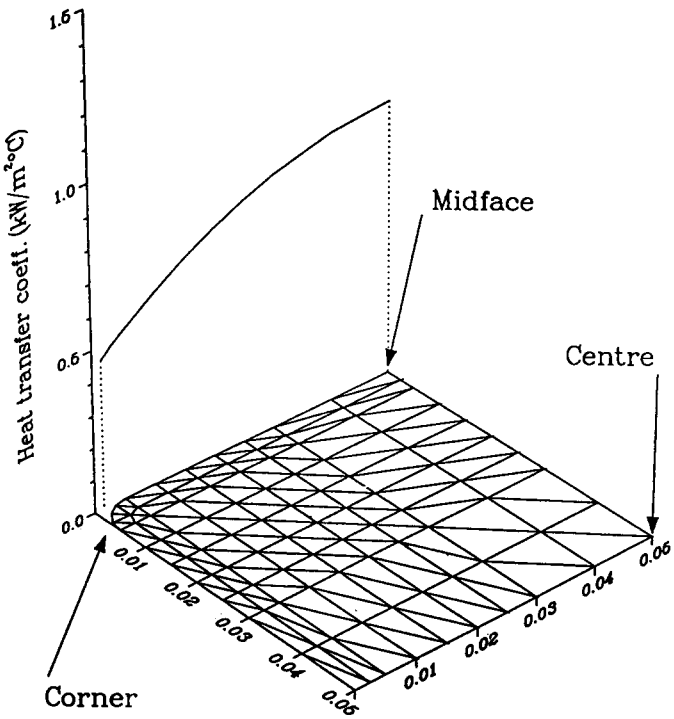

Fig. 4. Representation of the geometry and the approximation of boundary data at a fixed time.

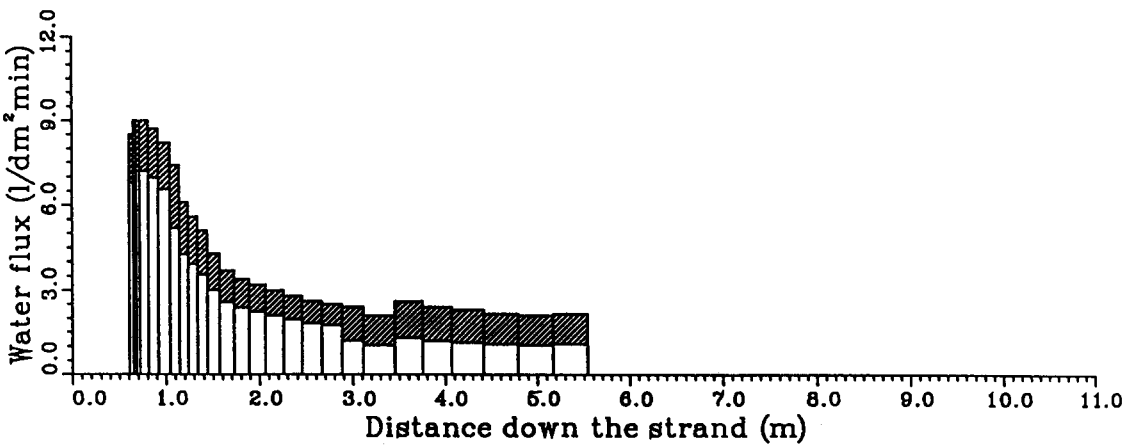

Fig. 5. Water flux distribution as a function of distance.

Figure 7 presents the calculated temperature distribution in three points (see Fig. 4) of the billet's cross-section.

In the above example we have assumed that the water-flux distribution in the withdrawal direction alters quite smoothly. However, this is not necessarily the case in practice. Due to the complexity of secondary cooling system (support rolls, spray-nozzle gaps etc.) the water-flux distribution may be as in Figure 8, where the nozzle-to-nozzle distances are long and there can be found undercooled regions between the sprays.

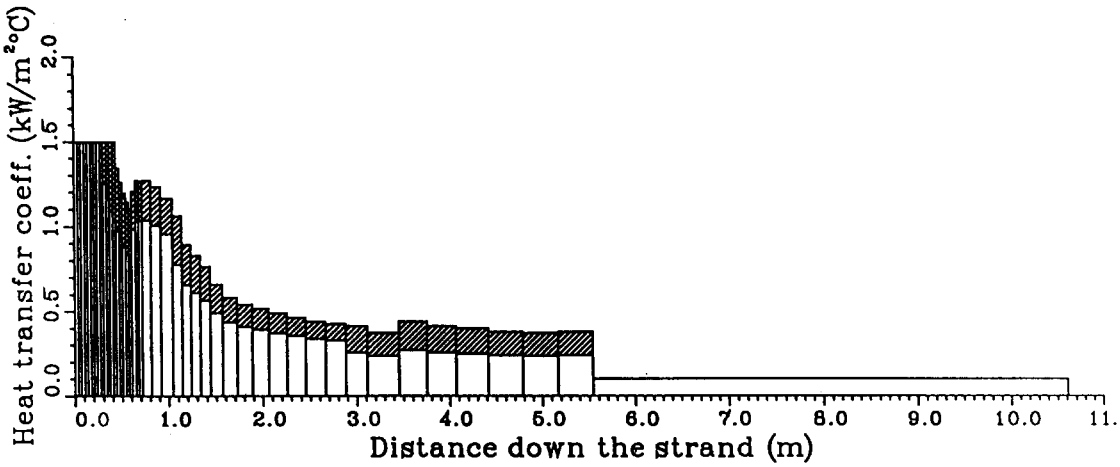

Fig. 6. Heat-transfer coefficients as a function of distance.

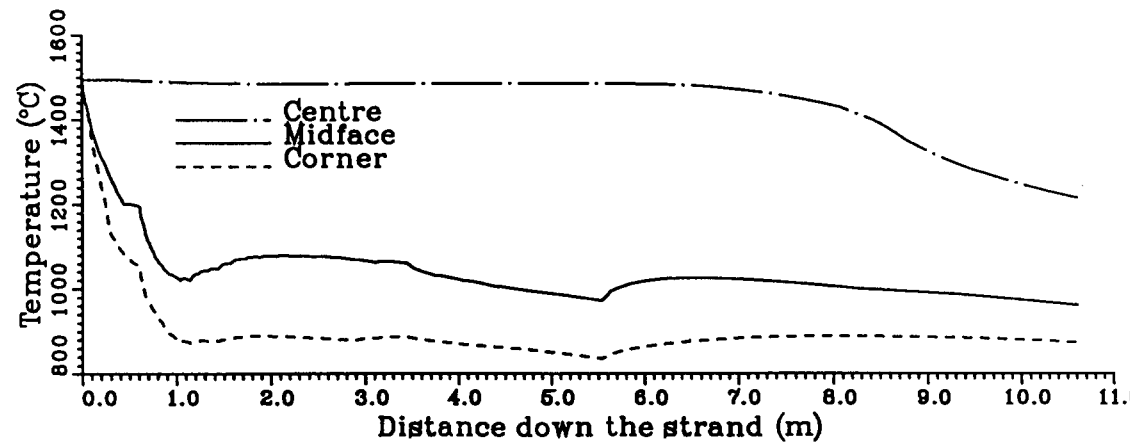

Fig. 7. The calculated temperature distribution in corner, midface and centre of billet's cross-section as a function of distance.

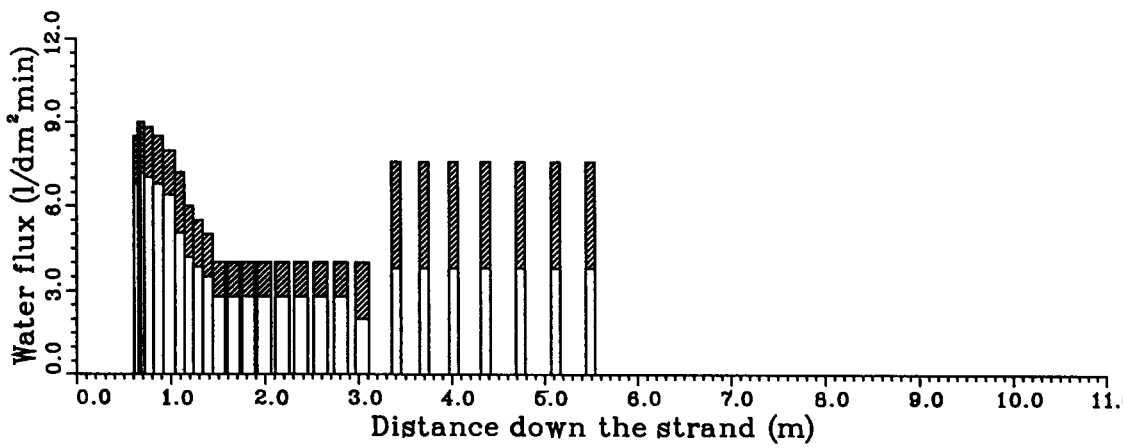

Fig. 8. Water-flux distribution as a function of distance.

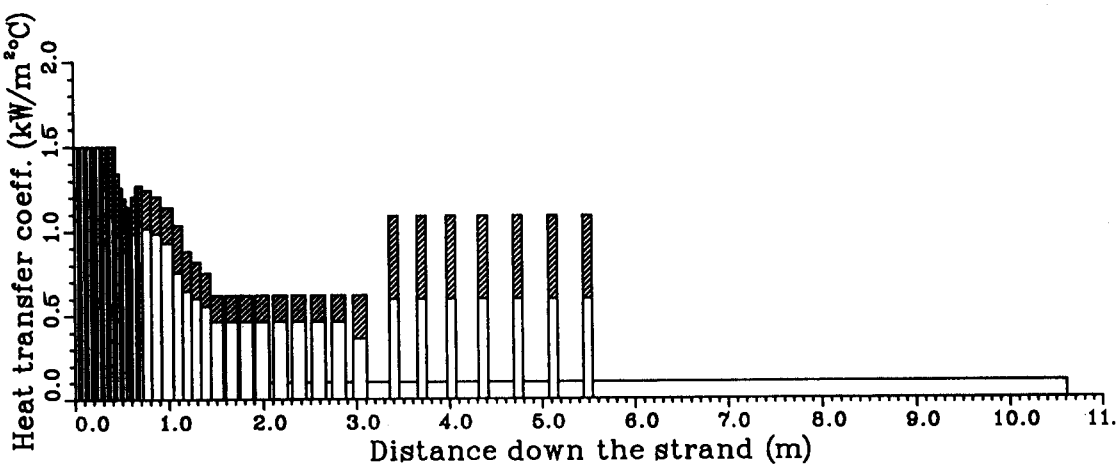

Fig. 9. Heat-transfer coefficients as a function of distance.

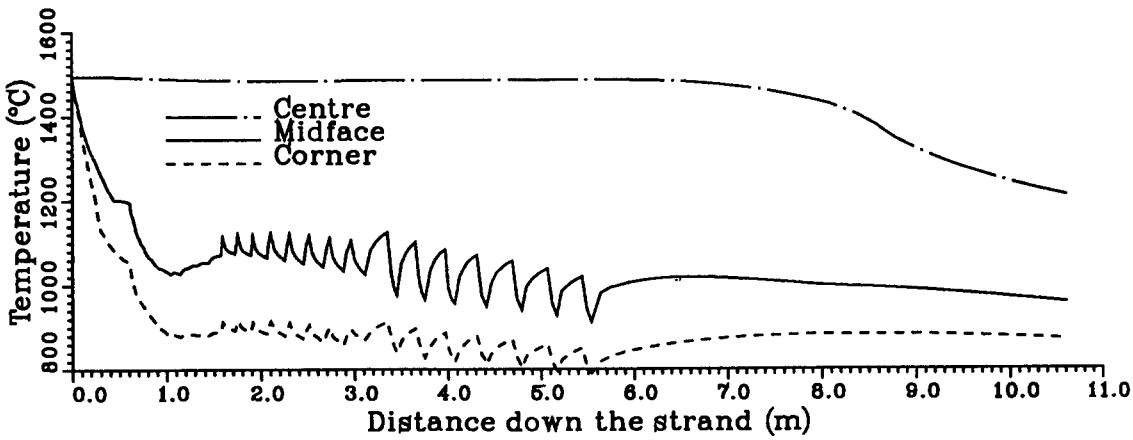

Fig. 10. The calculated temperature distribution in corner, midface and centre of billet's cross-section as a function of distance.

The corresponding heat-transfer coefficients related by equation (35) are shown in Figure 9 and the calculated surface temperature in the corner and midface of billet's cross-section and the centreline temperature are presented in Figure 10. In Figure 10 the surface temperature seems to oscillate quite a lot. However, this does not cause bad defects in the strand because the depth of oscillation is not deep and the solidified shell does not easily crack.

7. A rough algorithm to determine the water flux

We use the temperature model (11)–(13) inversely, too. We pose a question: *How should one choose the water-flux values on the surface to achieve a desired surface temperature along the secondary cooling region?*

To give an answer to this question we replace in the model (11)–(13) the Neumann boundary condition (12) in region $[t_1, t_2]$ by a Dirichlet boundary condition which defines the desired surface temperature. When the temperature distribution in the strand is solved, we use the flux condition on the surface to solve the heat-transfer coefficients and some related relation for solving the corresponding water-flux values. The algorithm for solving water-flux values is given below.

ALGORITHM 2:

STEP 1. For a given surface temperature T_g solve the problem (11)–(13) with the Dirichlet boundary data

$$T = T_g \quad \text{on } \Gamma \times [t_1, t_2].$$

STEP 2. Determine the strand heat-transfer coefficient h from the relation

$$-k(T)\frac{\partial}{\partial n}T = h(T - T_{H_2O}) + \sigma\varepsilon(T^4 - T_{ext}^4) \quad \text{on } \Gamma \times [t_1, t_2].$$

STEP 3. Determine the water flux W from relation (35) (or from some other similar relation).

In fact, we can solve the relation between water flux W and heat-transfer coefficient h by applying this algorithm and using the factory-measured surface temperature as a boundary condition.

The desired surface temperature T_g is given on the corner and midface by the equation

$$T_g(x, t) = \begin{cases} -1.53 \times t + 1212.18, & t \in [t_1, t_2] \text{ (corner)}, \\ -1.42 \times t + 1050.49, & t \in [t_1, t_2] \text{ (midface)}. \end{cases} \tag{36}$$

For the other points of Γ, T_g is given by the parabolic fitting.

In Figure 11(a) we see the desired boundary temperature along the secondary cooling region and in Figure 11(b) the corresponding water-flux distribution, calculated by the above algorithm. To verify the results we have solved the problem (11)–(13) with the boundary data as in Figure 11(b). In Figure 12(a) we present the calculated surface temperature and in 12(b) the calculated center-plane temperature. By comparing Figures 11(a) and 12(a) we find that the surface temperatures are almost the same.

8. Conclusions

Above we have presented and tested two algorithms. The first one is designed to determine the temperature distribution of the strand when the heat-transfer coefficient (or water flux) along the secondary cooling region is given. The second algorithm solves the inverse problem: which are the cooling conditions by which the desired surface temperature is attained?

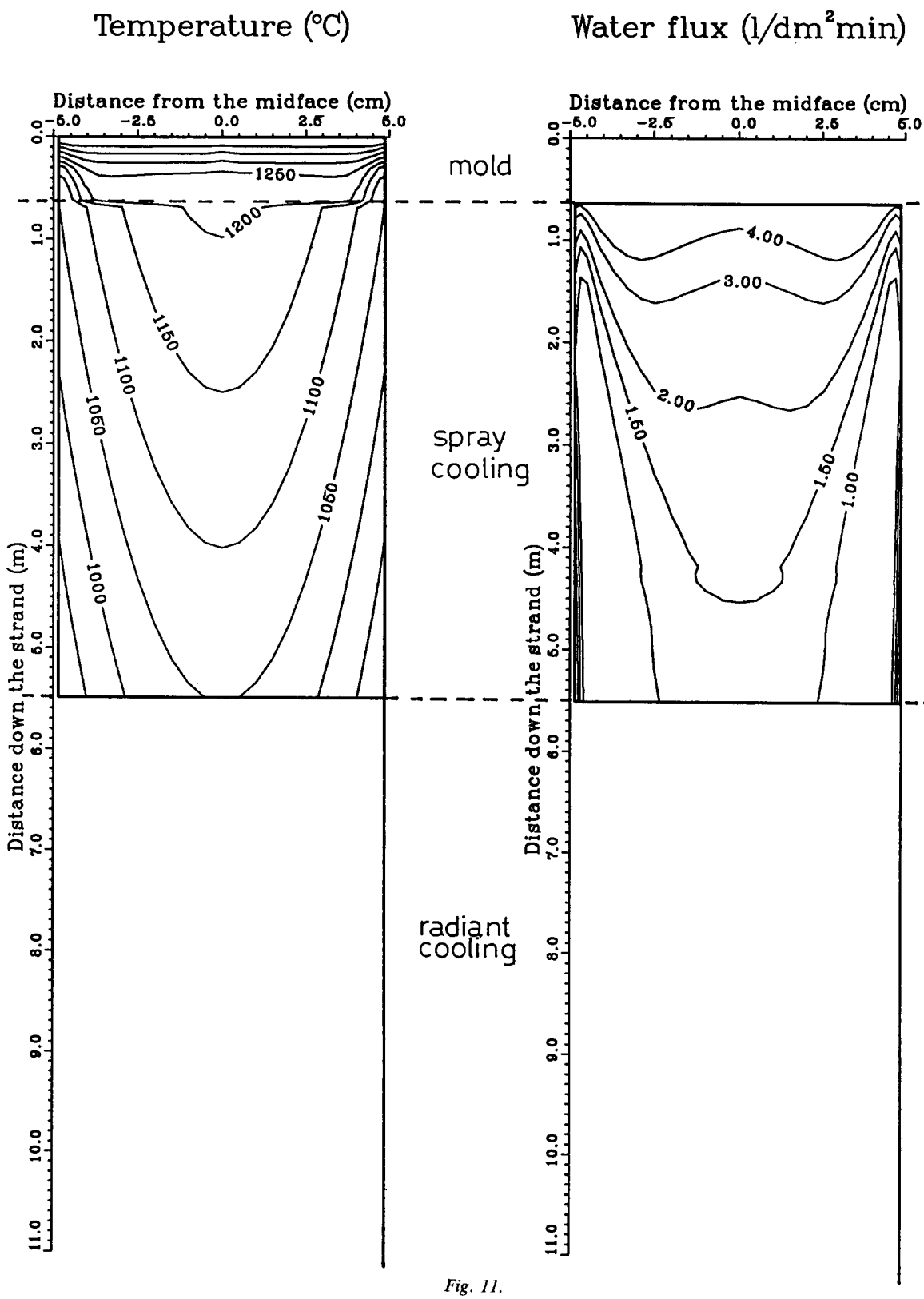
Temperature (°C)
Water flux (l/dm²min)
Distance from the midface (cm)
-5.0
-2.5
0.0
2.5
5.0
mold
spray cooling
radiant cooling
Distance down the strand (m)
0.0
1.0
2.0
3.0
4.0
5.0
6.0
7.0
8.0
9.0
10.0
11.0
1250
1200
1150
1100
1050
1000
4.00
3.00
2.00
1.50
1.00

Fig. 11.

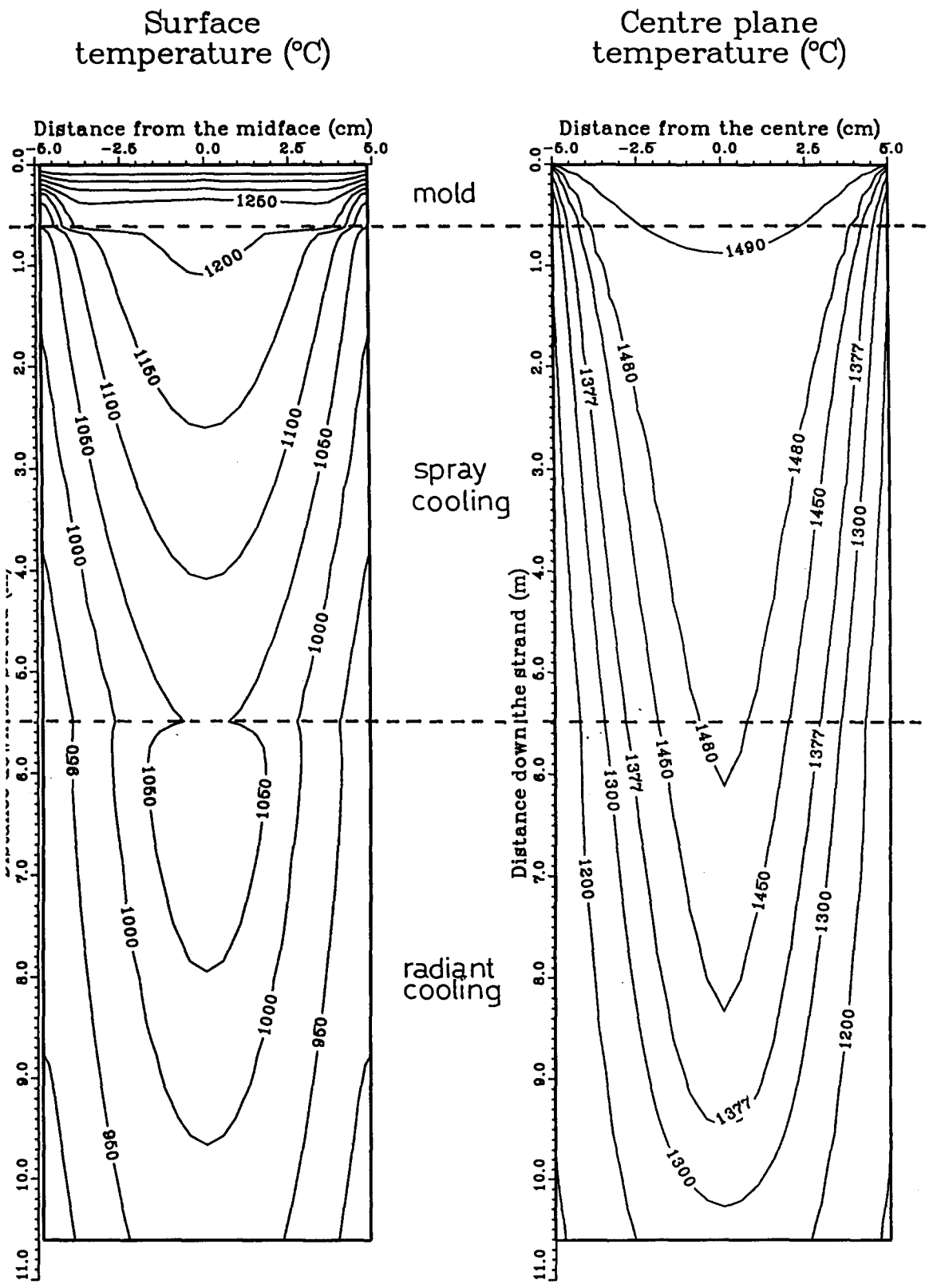
Surface temperature (°C)
Centre plane temperature (°C)
Distance from the midface (cm)
Distance from the centre (cm)
-5.0
-2.5
0.0
2.5
5.0
mold
spray cooling
radiant cooling
Distance down the strand (m)
0.0
1.0
2.0
3.0
4.0
6.0
7.0
8.0
9.0
10.0
11.0
1250
1200
1160
1100
1050
1000
950
900
1490
1480
1450
1377
1300
1200

Fig. 12.

Acknowledgements

This research was supported by TEKES (Technology Development Centre). The authors are indebted to T. Männikkö for his assistance in the graphical representation of numerical results by DISSPLA.

References

1. Brimacombe, J.K., Samareskera, I.V. and Lait, J.E., *Continuous Casting*, Book Crafters, Inc., Chelsea, MI (1984).
2. Danilyuk, I.I., On the Stefan problem, *Russian Math. Surveys* 40 (1985) 157–223.
3. Friedman, A., The Stefan problem in several space variables, *Trans. AMS* 133 (1986) 51–78.
4. Hong, C.P., Umeda, T. and Kimura, Y., Numerical methods for casting solidification. Part I: The coupling of the boundary element and finite difference methods for solidification problems, *Metallurgical Transactions* 15B (1984) 91–99.
5. Elliott, C.M., Error analysis of the enthalpy method for the Stefan problem, *IMA J. Numer. Anal.* 7 (1987) 61–71.
6. Elliott, C.M. and Ockendon, J.R., *Weak and variational methods for moving boundary problems*, Res. Notes Math., Pitman, Boston (1982).
7. Koikkalainen, P., Asano, N. and Neittaanmäki, P., Numerical modelling of material properties in mushy zone (in Japanese), to appear.
8. Lait, J.E., Brimacombe, J.K. and Weinberg, F., Mathematical modelling of heat flow in the continuous casting of steel, *Ironmaking and steelmaking* 2 (1974) 90.
9. Neittaanmäki, P., On the control of cooling during continuous casting, in: *Proc. of the 4th Int. Conf. on Numerical Methods in Thermal Problems*, July 15–18, 1985 in Swansea, Lewis, R.W. and Morgan, K. (Eds.), Pineridge Press (1986) 240–249.
10. Neittaanmäki, P. and Laitinen, E., Temperature distribution and its control, *GAMM, ZAMM* 66(4/6) (1986).
11. Niezgodka, M., Pavlow, I. and Visintin, A., On multi-phase Stephan type problems with nonlinear flux at the boundary in several space variables, *Pubb. N.* 293 (1981) Pavia.
12. Nochetto, R.H., A note on the approximation of free boundaries by finite element methods, *RAIRO Modél. Math. Anal. Numér.* 20 (1986) 355–368.
13. Pavlow, I., Analysis and control of evolution multi-phase problems with free boundaries, Prace habilitacyjne, Polska akademia Nauk (1987).
14. Rogberg, B., High temperature properties of steel and their influence on the formation of defects in continuous casting, Dissertation, The Royal Institute of Technology, Department of Casting of Metals (1982).
15. Tao, N.L., A method for solving boundary problems, *SIAM J. Appl. Math.* 46 (1986) 254–264.
16. Verdi, C. and Visintin, A., Error estimates for a semi-explicit numerical scheme for Stefan-type problems, submitted to *Numer. Math.*
17. Voller, V.R., Implicit finite-difference solutions of the enthalpy formulation of Stefan problems, *IMA J. Numer. Anal.* 5 (1985) 201–214.
18. Voller, V.R., Cross, M. and Markatos, N.C., An enthalpy method for convection/diffusion phase change, *Int. J. Numer. Meth. Eng.* 24 (1987) 271–284.
19. White, R. E., A nonlinear parallel algorithm with application to the Stefan problem, *SIAM J. Numer. Anal.* 23 (1986) 639–652.
20. Winzell, B., Finite element Galerkin method for multiphase Stefan problems, *Appl. Math. Modelling* 7 (1983) 329–344.